Dlg1 binds GKAP to control dynein association with microtubules, centrosome positioning, and cell polarity

Jean-Baptiste Manneville,[1] Muguette Jehanno,[2] and Sandrine Etienne-Manneville[2]

[1]UMR144 Centre National de la Recherche Scientifique-Institut Curie, Paris 75248, Cedex 05, France
[2]Institut Pasteur, Cell Polarity and Migration Group and Centre National de la Recherche Scientifique URA 2582, 75724 Paris, Cedex 15, France

Centrosome positioning is crucial during cell division, cell differentiation, and for a wide range of cell-polarized functions including migration. In multicellular organisms, centrosome movement across the cytoplasm is thought to result from a balance of forces exerted by the microtubule-associated motor dynein. However, the mechanisms regulating dynein-mediated forces are still unknown. We show here that during wound-induced cell migration, the small G protein Cdc42 acts through the polarity protein Dlg1 to regulate the interaction of dynein with microtubules of the cell front. Dlg1 interacts with dynein via the scaffolding protein GKAP and together, Dlg1, GKAP, and dynein control microtubule dynamics and organization near the cell cortex and promote centrosome positioning. Our results suggest that, by modulating dynein interaction with leading edge microtubules, the evolutionary conserved proteins Dlg1 and GKAP control the forces operating on microtubules and play a fundamental role in centrosome positioning and cell polarity.

Introduction

The ability of cells to polarize in a given direction upon extracellular or intracellular cues is essential for most cellular activities. Cell division, cell differentiation, cell migration, or T cell responses all require the generation of a polarity axis along which cytoskeletal elements and intracellular trafficking must be organized to function in a coordinated manner. The centrosome, which, in most eukaryotic cells, corresponds to the microtubule organizing center, plays a central role in the organization of the microtubule network, in the localization and function of intracellular trafficking, and in the maintenance of the cell internal architecture (Manneville and Etienne-Manneville, 2006; Tolić-Nørrelykke, 2008). Directed membrane trafficking and microtubule assembly into higher ordered structures such as spindles in cell division are crucial for most eukaryotic cell functions (Kirschner and Mitchison, 1986; Hyman and Karsenti, 1996). As a consequence, precise positioning of the centrosome is essential during symmetric and asymmetric cell division (Segal and Bloom, 2001; Cowan and Hyman, 2004; Corellou et al., 2005) and during differentiation of polarized cells such as epithelial cells or neurons (de Anda et al., 2005; Siegrist and Doe, 2006). In interphase cells, the centrosome is generally located near the cell center and its position relative to the nucleus is a good indicator of the cell polarity axis. The centrosome is positioned above the nucleus in baso-apically polarized epithelial cells and in front of the nucleus in the direction of the immune synapse during T cell response (Stinchcombe et al., 2006). In many cell types, including fibroblasts and astrocytes, the orientation of the nucleus–centrosome axis indicates the direction of migration (Yvon et al., 2002).

The mechanisms mediating centrosome positioning have received a great attention in the past decade and several in vitro and cellular models have been used to investigate the role of centrosome-bound microtubules in providing mechanical forces allowing centrosome movement. Depending on the system, microtubule-mediated pushing or pulling forces have been involved in centrosome positioning (Dogterom et al., 2005;

J.-B. Manneville and M. Jehanno contributed equally to this paper.

Correspondence to Sandrine Etienne-Manneville: sandrine.etienne-manneville@pasteur.fr

Abbreviations used in this paper: APC, adenomatous polyposis coli; DHC, dynein heavy chain 1; DIC, dynein intermediate chain; DLC, dynein light chain; GUK, guanylate kinase–like; IRM, interference reflection microscopy; TIRF, total internal reflection fluorescence.

The Rockefeller University Press $30.00
J. Cell Biol. Vol. 191 No. 3 585–598
www.jcb.org/cgi/doi/10.1083/jcb.201002151

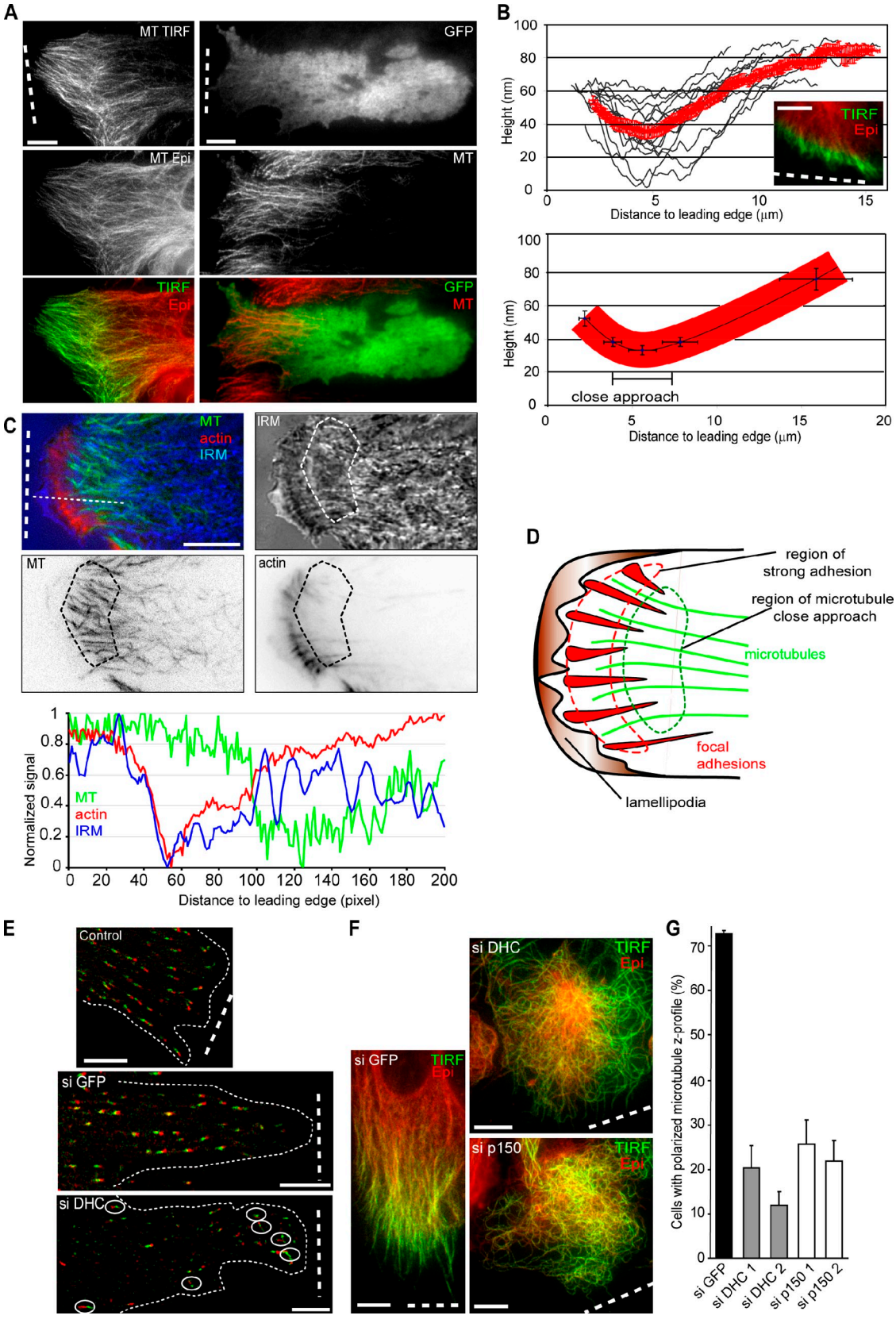

Figure 1. **The dynein–dynactin complex controls microtubule dynamics and the polarized approach of microtubules at the leading edge plasma membrane of migrating astrocytes.** (A) Superimposition of microtubule staining visualized by TIRF (green) and wide-field epifluorescence (red, left panels), and TIRF images of microtubules (red) in cytoplasmic GFP-expressing cells (right panels). Microtubules specifically approach the basal plasma membrane at the front of migrating cells independently of plasma membrane adhesion to the substrate. (B) Average (red) and individual microtubule z-profiles (black) in a migrating astrocyte (top graph). The inset shows the cell from which 16 individual microtubule z-profiles were calculated and analyzed. Cell-averaged microtubule morphology in migrating astrocytes (bottom graph). 6 cells were analyzed (see Materials and methods). Note the difference in scale between

Vallee and Stehman, 2005; Manneville and Etienne-Manneville, 2006; Tolić-Nørrelykke, 2008). Pushing forces essentially due to microtubule plus-end polymerization can promote centrosome centering in in vitro chambers (Holy et al., 1997; Faivre-Moskalenko and Dogterom, 2002) and spindle or nucleus in fission yeast (Tolić-Nørrelykke et al., 2004; Daga et al., 2006). However, in more complex and larger cell systems such as in the *Caenorhabditis elegans* zygote or in migrating cells, pulling forces exerted from the cell periphery have been shown to act on the centrosome. During asymmetric division of the *C. elegans* zygote, genetic or laser ablation of the mitotic spindle results in centrosome movement toward the cell poles (Grill et al., 2001, 2003; Cowan and Hyman, 2004; Grill and Hyman, 2005; Kimura and Onami, 2007). Similarly, in migrating fibroblasts, local depolymerization of the microtubule network induces centrosome movement away from depolymerizing microtubules (Burakov et al., 2003). These pulling forces can be induced by microtubule depolymerization or by microtubule-associated motors such as dynein.

Dynein is a microtubule minus end–directed motor involved in the establishment of a radial microtubule array (Koonce et al., 1999), in vesicular trafficking, ER and Golgi apparatus organization, and nucleus movement (Niclas et al., 1996; Reinsch and Karsenti, 1997; Wynshaw-Boris and Gambello, 2001; Allan et al., 2002; Tsai and Gleeson, 2005; Tolić-Nørrelykke, 2008). The dynein complex is built upon the association of several subunits including dynein heavy chains (DHCs), which form the motor domain, intermediate chains (DICs), and light chains (DLCs; King, 2003; Koonce and Samsó, 2004; Oiwa and Sakakibara, 2005). Dynein interaction with both microtubule plus ends and the cell cortex could generate a pulling force on the centrosome and thereby regulate centrosome positioning. In agreement with this hypothesis, dynein provides cortical anchors for microtubules and helps position spindles and nuclei in budding yeast (Eshel et al., 1993; Carminati and Stearns, 1997; Sheeman et al., 2003; Markus et al., 2009). Cytoplasmic dynein has been detected at the cortex of the *C. elegans* zygote and *Drosophila* oocytes (Li et al., 1994; Skop and White, 1998; Gönczy et al., 1999). During neuronal migration, cytoplasmic dynein is thought to be anchored at the plasma membrane in growth cones (Grabham et al., 2007), from where it promotes microtubule elongation and may also pull on the microtubules to move the centrosome forward (Solecki et al., 2004; Keays et al., 2007). Moreover, another pool of cytoplasmic dynein couples the microtubule network to the nucleus to promote nucleokinesis (Sasaki et al., 2000; Shu et al., 2004; Tanaka et al., 2004; Tsai et al., 2007). Dynein and its regulatory complex dynactin have also been shown to control centrosome positioning and polarity establishment during directed cell migration and immunological synapse formation (Etienne-Manneville and Hall, 2001; Palazzo et al., 2001; Gomes et al., 2005; Combs et al., 2006). In fibroblasts, dynein also accumulates at the leading edge during migration (Dujardin et al., 2003), consistent with a role of membrane-anchored microtubules in pulling the centrosome toward the front of migrating cells. However, the mechanisms by which the localization and activity of dynein or its partners are controlled during cell migration remain elusive.

Using a wound-induced migration assay that allows to control timing and directionality of cell movement and centrosome reorientation in front of the nucleus, we and others have previously shown that integrin engagement with the ECM at the leading edge of migrating cells induces a Cdc42-, Par6-, and PKC-ζ–dependent pathway that promotes centrosome reorientation (Etienne-Manneville and Hall, 2001; Palazzo et al., 2001; Gomes et al., 2005). PKC-ζ activation at the leading edge of migrating astrocytes induces adenomatous polyposis coli (APC) clustering at microtubule plus ends (Etienne-Manneville and Hall, 2003). Independently of APC clustering, Cdc42, Par6, and aPKC also promote the recruitment of the polarity protein Dlg1 (hDlg/SAP97) toward the leading edge (Etienne-Manneville et al., 2005). Interaction between APC and Dlg1 at the front of the cells controls microtubule network polarization, centrosome reorientation, and polarized alignment of microtubules in the elongated protrusions of migrating astrocytes (Etienne-Manneville et al., 2005). Here, we use wound-induced astrocyte migration to determine whether and how this polarity pathway may control dynein localization and function at the leading edge and to further characterize the molecular pathway responsible for centrosome positioning, microtubule network organization, and cell polarization.

Results

Leading edge microtubules bend down toward the lower plasma membrane

In astrocytes, like in fibroblasts, centrosome positioning depends on microtubule dynamics (Etienne-Manneville and Hall, 2001; Gomes et al., 2005), and in various models microtubule anchoring at the plasma membrane has been proposed to be responsible for centrosome positioning (Koonce et al., 1999; Manneville and Etienne-Manneville, 2006). To determine whether microtubules

the horizontal and vertical axes. (C) Combined dual-color TIRF microscopy and IRM (interference reflection microscopy) of a migrating astrocyte. Superimposition of IRM image (blue), microtubule (green), and actin (red) stainings and individual channels (gray) are shown. In IRM, darker signals reflect strong cell adhesion to the substrate, whereas in TIRF the fluorescence increases close to the substrate. Note that the contrast was inverted in microtubule and actin TIRF images. The dashed region shows the region of microtubule close approach toward the plasma membrane. The graph plots the intensity profiles of the IRM image, the microtubule, and the actin stainings (inverted contrast) along a leading edge microtubule (dotted line) from the leading edge toward the cell body. (D) Drawing showing the relative positions of the lamellipodia, the actin-rich strong adhesion region, and the zone where microtubules approach in close proximity with the plasma membrane at the leading edge of a migrating astrocyte. (E) EB1 dynamics in control (Control and si GFP) and DHC-depleted (si DHC) cells. Two frames were superimposed: the first frame is color coded in green and the second frame (separated from the first one by a time interval, Δt = 1.6, 1.7, and 1.3 s for control, si GFP, and si DHC, respectively) is color coded in red. In control cells, red EB1 clusters position in front of the corresponding green EB1 cluster toward the cell leading edge. Abnormal EB1 dynamics in the DHC-depleted cell is shown in ellipses. See Videos 6–8. (F) Superimposition of TIRF (green) and wide-field epifluorescence (red) images of microtubules in control (si GFP, left), DHC-depleted (si DHC, top right), and $p150^{Glued}$-depleted (si p150, bottom right) cells. (G) Quantification of polarized microtubule z-profile. 54–329 cells from three independent experiments were scored. Error bars represent SEM. Dashed lines indicate the orientation of the wound. Bars, 5 µm.

approach the plasma membrane of migrating cells, we used total internal reflection fluorescence (TIRF) microscopy (Axelrod, 2001; Toomre and Manstein, 2001) to illuminate specifically microtubules present in the first 100–200 nm above the glass coverslip (see Materials and methods). We have previously shown that microtubules enter the evanescent wave field only in wound-edge migrating cells (Etienne-Manneville et al., 2005). In these cells, only leading edge microtubules entered the evanescent wave field (Fig. 1 A). The TIRF image of microtubules was not due to variation in cell adhesion to the substratum because cytoplasmic GFP was visible by TIRF throughout the cell footprint (Fig. 1 A), indicating that microtubules reach down toward the basal plasma membrane at the front of the cell protrusion. From quantification of the TIRF intensity (Fig. 1, A and B; Materials and methods), the z-profile of microtubules can be calculated (Krylyshkina et al., 2003). The averaged z-profile shows that microtubules reach down from the cell center toward the plasma membrane in a region that is ∼5 µm behind the leading edge (Fig. 1 B). From this region microtubules curl up such that microtubule plus-ends are on average ∼20 nm higher than the lowest point in the z-profile (Fig. 1 B). In the following, we refer to this organization of the microtubule cytoskeleton as a "polarized microtubule z-profile." Interestingly, microtubules appeared to grow from and shrink back to the region in closest contact with the plasma membrane in the direction of migration (Videos 1 and 2). Phase-constrast movies of the leading edge of migrating astrocytes suggested that the region where microtubules reach toward the plasma membrane was located behind the lamellipodia, the extension of which is limited in astrocytes (Video 3). Interference reflection microscopy (IRM), which allows to visualize membrane adhesion to the substrate, confirmed the limited extension of the lamellipodia and showed that the lamellipodia is immediately followed by a region enriched in focal adhesions appearing as dark patches in IRM images (Video 4). To better localize where microtubules bend toward the plasma membrane with respect to the actin machinery, we compared the IRM signal with the fluorescence intensity of microtubule and microfilament stainings visualized by TIRF (Fig. 1 C). The IRM signal strongly correlated with the actin staining, which by TIRF essentially highlights focal adhesions. In contrast, the increased fluorescence of microtubules, corresponding to their close approach to the basal membrane, did not correlate with increased adhesion and localized behind the actin-rich adhesive zone, with a few microtubules extending between focal adhesions toward the leading edge (Fig. 1, C and D).

From polarized microtubule z-profiles, we can deduce an order of magnitude of the forces involved in microtubule bending toward the lower plasma membrane. The bending moment M of a microtubule is given by: $M = EI/R$, where R is the microtubule curvature and EI is the flexural rigidity (Felgner et al., 1996). The force required to deflect a microtubule of a distance d is thus $F = EI/(Rd)$. Taking d = 100 nm and R = 10 µm from the cell-averaged microtubule z-profile, and $EI \sim 1–10\ 10^{-24}\ Nm^2$ (Felgner et al., 1996), we find a force of ∼1–10 pN, responsible for microtubule bending near the plasma membrane. Similar forces are produced by molecular motors, suggesting that motor proteins could impose a mechanical tension on microtubules to hold them down in close proximity to the basal plasma membrane.

Dynein shapes microtubule z-profiles near the basal plasma membrane

Because cytoplasmic dynein is crucial for centrosome reorientation (Etienne-Manneville and Hall, 2001; Palazzo et al., 2001; Dujardin et al., 2003), we investigated the role of cytoplasmic dynein in shaping microtubule z-profiles at the leading edge of migrating cells. Primary astrocytes were nucleofected with two distinct siRNAs to inhibit the expression of DHC 1 (Fig. S1 A, 60% inhibition with siDHC 1, 40% inhibition with siDHC 2). In addition to DHC depletion, both siRNAs had a strong effect on DIC expression levels both by Western blot analysis and by immunofluorescence (Fig. S1 A, 92% inhibition with siDHC 1, 94% inhibition with siDHC 2; and Fig. S1 E), probably because these two molecules are part of the same molecular complex, contributing to their stability. In contrast, these siRNAs had no effect on β-catenin (Fig. S1 A). As previously described (Dujardin et al., 2003), inhibition of DHC expression strongly perturbed centrosome reorientation (Fig. S2, A, B, and D). In DHC-depleted cells, the Golgi apparatus was dispersed (Harada et al., 1998; Roghi and Allan, 1999) and also failed to localize in front of the nucleus after wounding (Fig. S2, A, C, and E). In these conditions, microtubule dynamics was dramatically perturbed precluding analysis from tubulin-GFP–expressing cells (Video 5). To analyze microtubule dynamics in dynein-depleted cells, we used astrocytes expressing EB1-GFP (Fig. 1 E and Videos 6–8). EB1 interacts specifically with the plus ends of growing microtubules, allowing visualization of microtubule growth. In control cells or in siGFP-transfected cells, microtubule plus-ends continuously grew from the cell center toward the leading edge (Videos 6 and 7; Fig. 1 E, control and siGFP). At the leading edge the EB1 clusters disappeared, indicating that microtubules undergo depolymerization as they come close to the leading edge cell cortex. Quantitative analysis of the direction of EB1 movement at the front of the cell showed that EB1 moves mainly perpendicularly to the leading edge (Fig. S3 A). In contrast, in DHC-depleted cells, the EB1 clusters did not disappear at the leading edge but moved along the plasma membrane and either turned along bent trajectories or moved back toward the cell body (Video 8 and Fig. 1 E, siDHC). This resulted in much less directed EB1 motion (Fig. S3 A). EB1 dynamics indicate that in the absence of dynein, microtubules do not stop growing when they contact the leading edge but instead buckle and turn around at the cell front, eventually growing back toward the cell center. Quantification of abnormal microtubule behavior showed that approximately half of the microtubules were not stopping at the leading edge and kept polymerizing (Fig. S3 B). A similar abnormal microtubule behavior has been observed recently in cells lacking EB3 (Straube and Merdes, 2007) or tubulin tyrosine ligase (Peris et al., 2009) and was interpreted as a lack of microtubule capture or anchoring at the cell cortex. As a consequence, the microtubule network was strongly disorganized. Buckled microtubules were visible in the evanescent field throughout the cell footprint, leading to a nonpolarized microtubule z-profile (Fig. 1, F and G). Depletion of the $p150^{Glued}$ subunit of dynactin

by two different siRNA sequences (Fig. S1 B) had the same effects as DHC depletion (Fig. 1 G and Fig. S2), further confirming the role of dynein in the regulation of microtubule dynamics and organization at the cell leading edge and in cell orientation.

Dynein association with microtubules requires Cdc42 and Dlg1

To study the regulation of dynein during cell migration, we first analyzed the localization of dynein in migrating astrocytes. Immunofluorescence using anti-DIC antibodies showed that dynein is concentrated at the centrosome and localizes along microtubules (Fig. 2, A and B). TIRF microscopy revealed that dynein is present along the leading edge microtubules that bend down toward the basal plasma membrane in migrating cells (Fig. 2 C). Quantification of dynein colocalization with microtubules in TIRF images indicated that 53 ± 3% of dynein signal localized on microtubules. Random superimposition of the dynein and microtubule images resulted in a drop in dynein–microtubule colocalization to 18 ± 1%, corresponding to random colocalization of the two stainings (see Materials and methods). For comparison, only 25 ± 1% of the focal adhesion–associated protein vinculin colocalized with microtubules. Fig. 2 D shows normalized colocalization values of DIC and vinculin on microtubules (see Materials and methods).

The small G protein Cdc42 plays an essential and conserved role in the regulation of cell polarity in various systems (Etienne-Manneville, 2004). Upon wounding, Cdc42 is recruited and activated at the wound edge of astrocytes (Etienne-Manneville and Hall, 2001). Cdc42-localized activation is required for dynein-dependent centrosome reorientation (Etienne-Manneville and Hall, 2001). Cdc42 depletion using specific siRNAs (Fig. S1 C; Osmani et al., 2006) perturbed dynein localization. In the cell protrusion, dynein colocalization with microtubules was decreased threefold in Cdc42-depleted cells (Fig. 2, E and F). We have previously shown that Cdc42 regulates centrosome positioning by recruiting and activating a Par6–aPKC complex, which, in turn, is responsible for both APC clustering at microtubule plus-ends and Dlg1 (hDlg/SAP97) recruitment along microtubules near the cell leading edge (Fig. 7; Etienne-Manneville and Hall, 2003; Etienne-Manneville et al., 2005). We thus tested whether these downstream targets of Cdc42 were involved in dynein recruitment to leading edge microtubules. siRNA-induced depletion of APC (Etienne-Manneville et al., 2005) had a small but detectable effect on DIC localization (Fig. 2 F). The effects of Dlg1 depletion by siRNA (Etienne-Manneville et al., 2005) were much stronger, as it led to a twofold decrease in DIC colocalization with microtubules (Fig. 2, E and F), strongly suggesting that Dlg1 is a major downstream effector of Cdc42 to control dynein interaction with microtubules. In contrast, EB1 depletion by siRNA (Fig. S1 D), which affects microtubule dynamics and polarization (Etienne-Manneville et al., 2005; Komarova et al., 2009), did not alter dynein interaction with leading edge microtubules (Fig. 2, E and F). Inhibition of dynein recruitment to microtubules in Dlg1-depleted cells correlated with abnormal EB1 motion near the leading edge and microtubule dynamics (Fig. S3). Like in DHC-depleted cells, microtubules grew continuously and buckled along the leading edge plasma membrane (Video 9 and

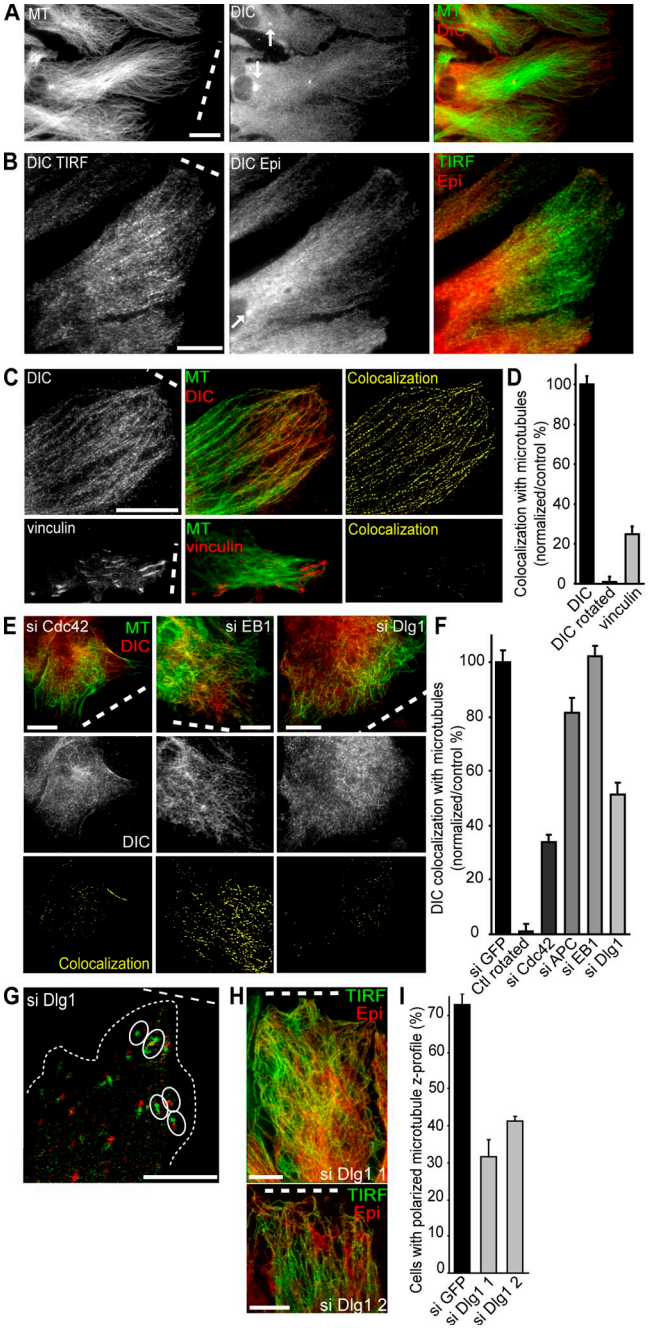

Figure 2. **Cdc42 and Dlg1 are required for dynein localization along microtubules.** (A) Localization of DIC by epifluorescence. DIC (red) concentrates at the centrosome and along microtubules (green). (B) Superimposition of DIC staining visualized by TIRF (green) and wide-field epifluorescence (red). (C) DIC (red, top panels), but not vinculin (red, bottom panels), aligns along microtubules (green) in TIRF images. Colocalization is shown in yellow (see Materials and methods). (D) Quantification of colocalization of DIC and vinculin on microtubules (see Materials and methods). (E) TIRF images showing DIC or DIC (red) and microtubules (green) in cells nucleofected with the indicated siRNA. Colocalization is shown in yellow (bottom panels). (F) Quantification of colocalization of DIC on microtubules in cells treated with the indicated siRNAs. (G) EB1 dynamics in Dlg1-depleted cells. Abnormal EB1 dynamics are shown in ellipses. The second frame (red) is separated from the first one (green) by a time interval, Δt = 1.9 s. See Video 9. (H) Superimposition of TIRF (green) and wide-field epifluorescence (red) images of microtubules in Dlg1-depleted cells. (I) Quantification of polarized microtubule z-profile. 206–294 cells from three independent experiments were scored. Error bars represent SEM. Arrows in A and B point to the centrosome region. Dashed lines indicate the orientation of the wound. Bars, 5 µm.

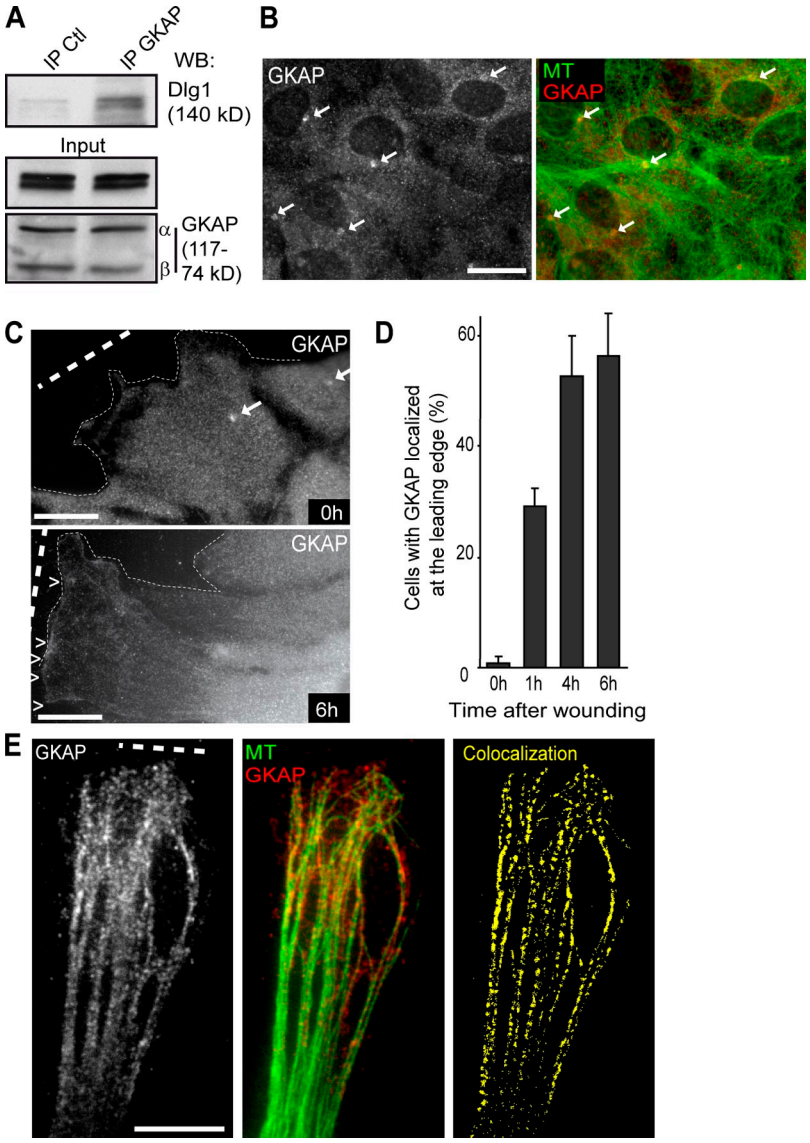

Figure 3. **GKAP binds Dlg1 and is recruited to leading edge microtubules after wounding.** (A) Astrocyte extracts were immunoprecipitated with anti-GKAP (IP GKAP) or irrelevant control (IP Ctl) antibodies. Immunoprecipitates and total cell lysates were analyzed by Western blotting (WB) using anti-GKAP and anti-Dlg1 antibodies. (B) Immunofluorescence of GKAP (red) and microtubules (green) in confluent, nonmigrating astrocytes. (C) GKAP immunostaining in astrocytes 0 and 6 h after wounding. GKAP is recruited to the leading edge of migrating cells (arrowheads). Dotted lines show cell edges. (D) Quantification of GKAP recruitment to the cell leading edge 0, 1, 4, and 6 h after wounding. Results are shown as mean ± SEM of 300 cells from three independent experiments. (E) TIRF images of GKAP (red) and microtubule (green). Colocalization is shown in yellow (right panels). Arrows in B and C point to the centrosome region. Dashed lines indicate the orientation of the wound. Bars: (B and C) 10 µm; (E) 5 µm.

Fig. 2 G), resulting in a disorganized microtubule cytoskeleton and nonpolarized microtubule z-profiles (Fig. 2, H and I).

Dlg1 binds GKAP and controls its recruitment to leading edge microtubules

To understand how Dlg1 may regulate dynein localization on microtubules, we investigated the role of GKAP (also called DLGAP-1, SAPAP-1, or DAP-1). GKAP is a member of the SAPAP family identified for its ability to directly interact with the guanylate kinase–like (GUK) domain of the SAP (Dlg) protein family (Kim et al., 1997; Kosako et al., 1997; Satoh et al., 1997; Fujita and Kurachi, 2000). The GKAP–Dlg1 interaction was confirmed by coimmunoprecipitation of overexpressed proteins in COS cells (Fig. S4). Although described as neuron-specific molecules, we could detect the two isoforms of GKAP (GKAP-α and GKAP-β) in primary astrocytes by Western blotting (Fig. 3 A). We confirmed the GKAP–Dlg1 interaction in primary astrocytes by coimmunoprecipitation of the endogenous proteins (Fig. 3 A). We then investigated the localization of GKAP during astrocyte polarization. Immunostaining revealed that, in confluent, nonmigrating astrocytes, GKAP localized mainly at the centrosome and in a perinuclear region (Fig. 3 B, arrows) and was barely visible in the cell periphery. During the first hours after wounding, GKAP was progressively recruited to the leading edge in a majority of wound-edge cells (Fig. 3, C and D). In migrating cells, GKAP localization at the centrosome often appeared fainter than in nonmigrating astrocytes. When visualized by TIRF microscopy in migrating cells, GKAP localized along leading edge microtubules (Fig. 3 E). Quantitative analysis, similar to that performed for DIC, showed that 47.1 ± 1.4% (n = 15 cells) of GKAP colocalized with microtubules.

We have previously shown that during astrocyte polarization, Dlg1 was recruited to the leading edge of migrating astrocytes and partially localized along leading edge microtubules and colocalized with APC at microtubule plus-ends (Etienne-Manneville et al., 2005). We used here a different antibody which also showed Dlg1 localization on microtubules, including at microtubule plus-ends, but the plasma membrane–associated staining described previously was less visible, probably due to variations in the epitope accessibility in these different locations.

By TIRF microscopy, both Dlg1 and GKAP were visible in the evanescent field, where they both appeared to colocalize along linear structures (Fig. 4 A) that probably correspond to leading edge microtubules, where GKAP was also found (Fig. 3 E). The specificity of Dlg1 and GKAP staining was confirmed using siRNA-transfected cells. siDlg1 (and siGKAP) led to a strong reduction in the immunofluorescence signal of Dlg1 (and GKAP, respectively; Fig. S1 E). We found that Dlg1 depletion dramatically altered wound-induced recruitment of GKAP to the leading edge (Fig. 4 B) and GKAP localization along leading edge microtubules (Fig. 4 C). Cdc42, which is involved in Dlg1 recruitment to the leading edge (Etienne-Manneville et al., 2005), was also required for GKAP localization (Fig. 4, B and C). In absence of Dlg1 or Cdc42, GKAP localization was restricted to a perinuclear and centrosomal area as in nonmigrating cells (Fig. 4 B). Collectively these results strongly suggest that, upon wounding, activation of Cdc42 leads to Dlg1 recruitment on leading edge microtubules. Dlg1 interacts with APC at microtubule plus-ends (Etienne-Manneville et al., 2005) and with GKAP along the microtubules, where APC is barely detected, to promote GKAP recruitment to microtubules of the cell protrusion (see Fig. 7).

GKAP mediates Dlg1 interaction with dynein

In addition to its binding to Dlg1, GKAP has been shown to interact with the dynein light chain LC8 (Rodríguez-Crespo et al., 2001). GKAP interaction with dynein was observed in astrocytes where GKAP coprecipitated with DIC (Fig. 5 A). Because GKAP can interact with both Dlg1 and dynein and also localizes on front edge microtubules during astrocyte migration, we tested whether the three molecules could be part of the same molecular complex. DIC was immunoprecipitated from astrocytes after wounding. Dlg1 coprecipitated with DIC. The Dlg1–DIC interaction slightly but reproducibly increased after wounding before decreasing back to normal levels after 6 h (Fig. 5 B). To assess the role of GKAP in this interaction, three different siRNA sequences were used successfully, respectively inhibiting GKAP expression by 72%, 56%, and 48% (Fig. 5 C). These siRNAs did not affect the expression levels of DIC and Dlg1 (Fig. 5, C and D). As a control we used an siRNA targeting GFP (si GFP) and a scramble version of the GKAP siRNA 3 (si Scramble). Cell transfection with GKAP siRNA led to a strong inhibition of DIC coimmunoprecipitation with Dlg1 (inhibition = 87% ± 11, $n = 3$), whereas control siRNAs had no effect (Fig. 5 D). These observations indicate that GKAP is required for the Dlg1–dynein interaction, suggesting that GKAP acts as a molecular bridge between Dlg1 and dynein. We then investigated whether GKAP was involved in Dlg1-dependent recruitment of dynein on leading edge microtubules. Similarly to Dlg1 depletion (Fig. 2, E and F), inhibition of GKAP expression interfered with dynein interaction with microtubules in the protrusion of migrating cells (Fig. 5, E and F).

GKAP is required for microtubule-polarized organization and centrosome reorientation

In agreement with a role of cytoplasmic dynein in shaping microtubule z-profiles and polarizing the microtubule network, GKAP depletion also strongly affected EB1 dynamics (Video 10, Fig. 6 A,

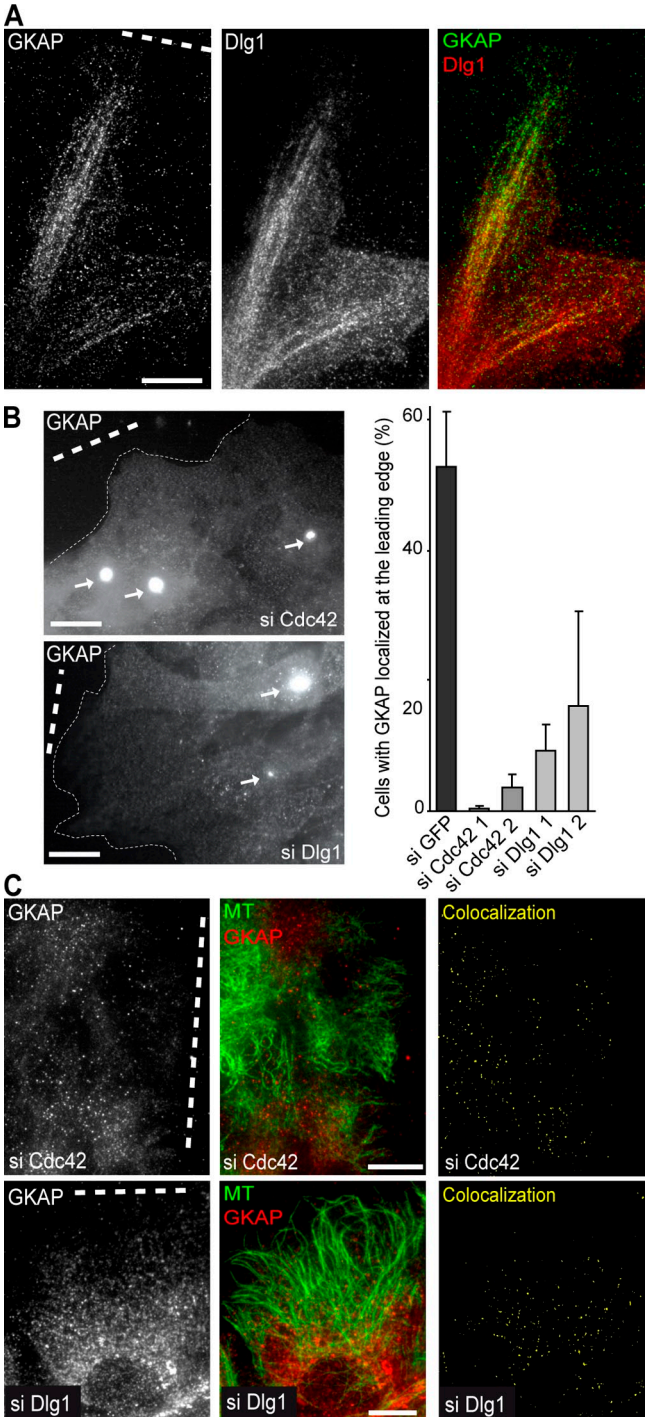

Figure 4. **Dlg1 controls GKAP recruitment to leading edge microtubules downstream of Cdc42.** (A) TIRF images showing Dlg1 (red) and GKAP (green). (B) Cdc42 or Dlg1 depletion inhibits GKAP recruitment to the cell leading edge. Immunofluorescence of GKAP after treatment with si Cdc42 or si Dlg1 (left) and corresponding quantification. Results are shown as mean ± SEM of 300 cells from three independent experiments. Arrows point to the centrosome. Dotted lines show cell edges. (C) TIRF images of GKAP or GKAP (red) and microtubules (green) in Dlg1- or Cdc42-depleted cells. Colocalization is shown in yellow (right panels). Dashed lines indicate the orientation of the wound. Bars, 5 µm.

and Fig. S3). Consequently, microtubule-polarized z-profile was dramatically altered in siGKAP-transfected cells (Fig. 6, B and C). Control siRNAs had no effect on polarized microtubule

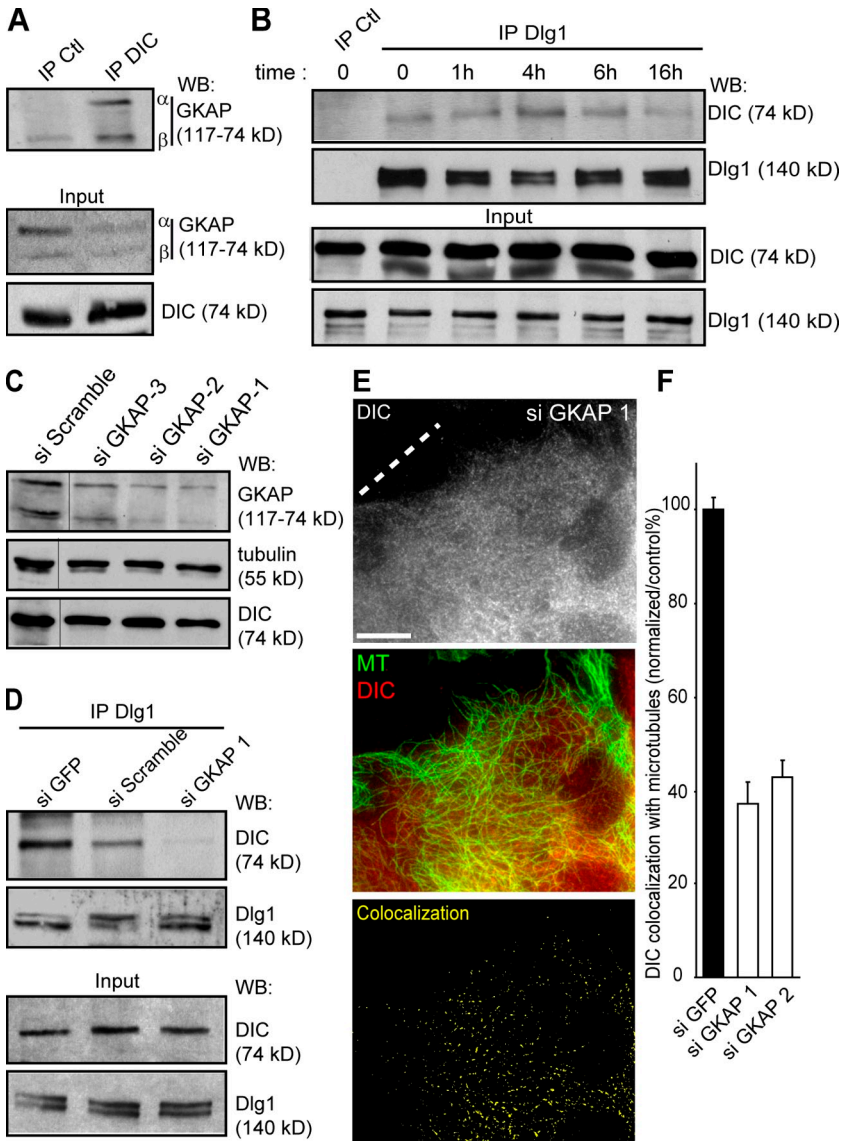

Figure 5. **GKAP interacts with DIC and is required for DIC interaction with Dlg1 and DIC recruitment to microtubules.** (A) Astrocyte extracts were submitted to immunoprecipitation with anti-DIC (IP DIC) or irrelevant control (IP Ctl) antibodies. Immunoprecipitates and total cell lysates were analyzed by Western blotting (WB) using anti-GKAP and anti-DIC antibodies. (B) Extracts from primary astrocytes were obtained at the indicated times after wounding. Lysates were subjected to immunoprecipitation with anti-Dlg1 (IP Dlg1) or irrelevant control antibody (IP Ctl). Immunoprecipitates and total cell lysates were analyzed by Western blotting (WB) using anti-DIC (top panels) and anti-Dlg1 antibodies (bottom panels). (C) Anti-GKAP, anti-tubulin, and anti-DIC Western blots of protein extracts from astrocytes 5 d after nucleofection by a control siRNA (si Scramble) and three different GKAP siRNAs (si GKAP 1, si GKAP 2, si GKAP 3). (D) Western blots showing DIC and Dlg1 in Dlg1 immunoprecipitates from astrocytes nucleofected with control (si GFP, si Scramble) or GKAP (si GKAP 1) siRNAs. (E) TIRF images showing DIC (top) or DIC (red) and microtubules (green) (middle) in GKAP-depleted cells. Colocalization is shown in yellow (bottom). (F) Quantification of colocalization of DIC on microtubules in astrocytes nucleofected with si GKAP 1 and si GKAP 2. Dashed lines indicate the orientation of the wound. Bars, 5 µm.

z-profile (Fig. 6, B and C; si GFP and si Scramble). Furthermore, expression of an siRNA-resistant GKAP construct rescued microtubule-polarized z-profile, further confirming the specific role of GKAP (Fig. 6, B and C; si GKAP 3 + GKAP).

Centrosome reorientation was also perturbed after GKAP depletion and expression of an siRNA-resistant GKAP construct rescued centrosome reorientation (Fig. 6, D and E; Fig. S5). In contrast, siGFP and siScramble had no effect on centrosome reorientation. To confirm the role of the Dlg1–GKAP interaction in cell polarization, we used constructs encoding the C-terminal GUK domain of Dlg1 (Dlg1 Cter and Dlg1 GUK), which is responsible for Dlg1 interaction with an N-terminal region of GKAP (Fig. S4, A and B; Kim et al., 1997) to perturb endogenous Dlg1 binding to GKAP. A Dlg1 construct lacking the GUK domain (Dlg1 ΔGUK) was also used to compete with endogenous Dlg1 for leading edge recruitment. Microinjection of these different constructs led to a strong decrease in GKAP and DIC recruitment to microtubules (Fig. S4, D and E) and dramatically perturbed centrosome reorientation (Fig. 6 E and Fig. S5). To perturb the Dlg1–GKAP–dynein interaction, we overexpressed deletion mutants of GKAP that are no longer able to bind Dlg1 (GKAP ΔDlg BD) but could still bind dynein, or that cannot interact with DLC LC8 (GKAP ΔLC8 BD) (Rodríguez-Crespo et al., 2001) but still interact with Dlg1 (Fig. S4 C). Expression of these deletion mutants prevented DIC recruitment to leading edge microtubules, whereas expression of a full-length protein had no effect (Fig. S4 E). These constructs also inhibited wound-induced centrosome reorientation (Fig. 6 E), further confirming that the Dlg1–GKAP–dynein complex is essential for cell polarization. Collectively, our data show that GKAP mediates the interaction between Dlg1 and dynein and is involved in Cdc42- and Dlg1-dependent association of dynein with microtubules and, as a consequence, in dynein-dependent bending of leading edge microtubules toward the basal plasma membrane, centrosome reorientation and cell polarization.

Discussion

In interphase cells, the centrosome is generally maintained at the cell center. During directed migration of most cell types, the centrosome localizes in front of the nucleus to generate a

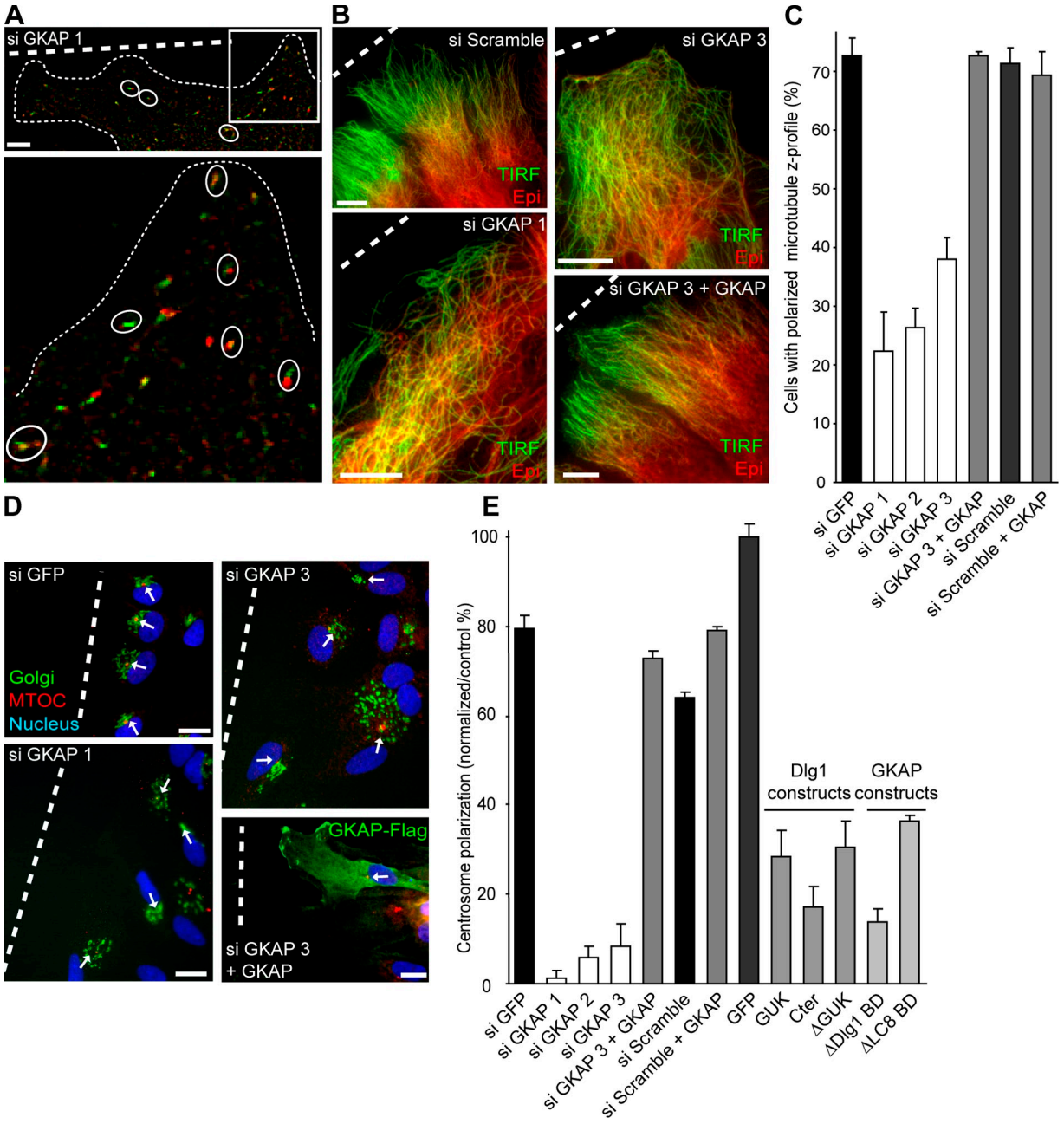

Figure 6. **GKAP is required for microtubule-polarized organization and dynamics and for centrosome reorientation.** (A) EB1 dynamics in GKAP-depleted cells. Abnormal EB1 dynamics is shown in ellipses. A zoom of the boxed region is shown on the bottom image. The second frame (red) is separated from the first one (green) by a time interval, Δt = 1.2 s. See Video 10. (B) Superimposition of TIRF (green) and wide-field epifluorescence (red) images of microtubules in control cells (si Scramble), in GKAP-depleted cells (si GKAP 1 and si GKAP 3), and in GKAP-depleted cells rescued by an siRNA-resistant GKAP construct (si GKAP 3 + GKAP). (C) Quantification of polarized microtubule z-profile. Results are shown as mean ± SEM of 300 cells from three independent experiments. (D) Golgi apparatus (green), centrosome (red), and nucleus (blue) were stained in control cells (si GFP) and GKAP-depleted cells (si GKAP 1 and si GKAP 3) and in GKAP-depleted cells rescued by an siRNA-resistant GKAP construct (si GKAP 3 + GKAP) using an anti-GM130 (green) antibody, an anti-pericentrin (red, white arrows) antibody, and Hoechst (blue). (E) Quantification of centrosome reorientation in siRNA-treated cells (control si GFP; si GKAP 1, 2, or 3; si GKAP 3 + GKAP; si Scramble; si Scramble + GKAP) and in microinjected cells (control GFP; Dlg1 constructs: GUK, Cter, and ΔGUK; GKAP constructs: ΔDlg1 BD and ΔLC8 BD). Dashed lines indicate the orientation of the wound. Bars: (A and B) 5 μm; (D) 10 μm.

polarized intracellular organization and moves forward to be maintained in front of the nucleus as the cells migrates. Centrosome movement during astrocyte migration requires microtubule dynamics and dynein (Etienne-Manneville and Hall, 2001; Fig. S2). We show here that dynein recruitment to the newly polymerized microtubules of the leading edge is controlled by a signaling pathway that is activated at the onset of migration. This pathway involves the small G protein Cdc42 and Dlg1, the orthologue of the Discs Large *Drosophila* protein, which interacts with dynein via GKAP. By regulating dynein association with microtubules, local activation of this pathway at the leading edge of the cell controls microtubule dynamics and organization at the cell front and forward movement of the centrosome (Fig. 7).

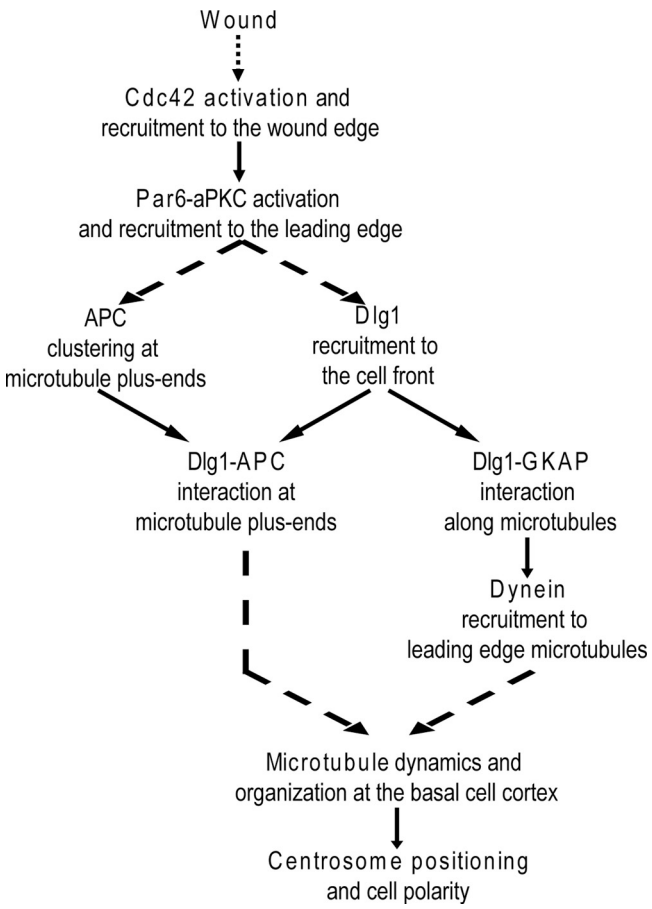

Figure 7. **Schematic diagram showing molecular pathways occurring at the leading edge of migrating astrocytes after wounding.** Upon wounding, integrin activation at the leading edge induces Cdc42 activation and recruitment at the wound edge (Etienne-Manneville and Hall, 2001; Osmani et al., 2006). Active Cdc42 binds and activates the Par6–aPKC complex, which in turn induces APC and Dlg1 recruitment to leading edge microtubules to promote centrosome reorientation (Etienne-Manneville and Hall, 2003; Etienne-Manneville et al., 2005). We show here that Dlg1 regulates dynein interaction with leading edge microtubules via GKAP and subsequent microtubule polarization and cell migration.

Current models of centrosome positioning involve a regulated balance of forces exerted on microtubules from the cell cortex. We show here using TIRF microscopy that in migrating astrocytes, microtubules approach the cell cortex in a region located just behind a focal adhesion–rich adhesive region, which lays a few micrometers behind the leading edge. Dynein controls the specific organization of the microtubule cytoskeleton at the leading edge by imposing a downward curvature of microtubules close to the basal plasma membrane and by regulating microtubule dynamics. These results strongly suggest that dynein participates in anchoring microtubules to the basal cell cortex. In the following discussion, microtubules entering the evanescent wave field at the front of the protrusion will be called "membrane-anchored" microtubules and the region where microtubules bend down toward the basal plasma membrane in a dynein-dependent manner will be referred to as the "anchoring" region.

Microtubule curvature toward the lower plasma membrane indicates that forces in the range of 1–10 pN mediate cortex–microtubule interactions. The microtubule portion in closest proximity to the membrane is ~3 µm away from the plus ends, showing that microtubules are not anchored at the cell cortex by their plus ends and arguing against an end-on attachment mechanism. In fact, we found that dynein is present along membrane-anchored microtubules. The anchoring region may provide a cortical site from which dynein may exert its minus-end activity and pull the centrosome in the direction of cell migration. In theory, the magnitude of dynein-generated forces on a single microtubule depends on the number of motors involved and thus on the size of the anchoring region and on the concentration of motors in the anchoring region. Our observations only show a slight enrichment in dynein in the anchoring region but clearly demonstrate that the extent and localization of this region is regulated during cell migration. Whether such a mechanism of microtubule anchoring at the cell cortex also plays a role in a 3D environment remains to be demonstrated. However, centrosome reorientation is a general phenomenon observed in cultured cells as well as in developing organisms, and dynein plays a key role in centrosome positioning in many systems (Manneville and Etienne-Manneville, 2006). Moreover, the signaling pathway controlling centrosome positioning during astrocyte migration depends on β1 integrin engagement with the ECM (Peng et al., 2008) and these integrins are expressed by astrocytes in vivo (Tawil et al., 1994), suggesting that the downstream signaling pathway is likely to be activated in vivo.

The force generated by dynein on microtubules could be modulated not only by dynein association with microtubules but also by regulating individual dynein activity. Lis1 and dynactin have been implicated in dynein function in migrating cells (Dujardin et al., 2003). Depletion of $p150^{Glued}$ leads to a severe disruption of microtubule organization comparable to dynein depletion. In addition, lack of $p150^{Glued}$ or of dynein dramatically inhibits cell migration (Dujardin et al., 2003). GKAP depletion had a similar effect. The role of the dynein–GKAP complex in cell migration may be uncoupled from its role in microtubule anchoring and centrosome positioning because depletion of Dlg1 induces a loss of microtubule anchoring and centrosome positioning but has only a moderate effect on cell migration (Etienne-Manneville et al., 2005). Dujardin et al. (2003) reported that dynein and dynactin also localize to an actin-rich zone corresponding to membrane ruffles at the leading edge of migrating fibroblasts, and may therefore be involved in actin regulation. The leading edge of migrating astrocytes shows a very limited lamellipodia (Etienne-Manneville and Hall, 2001). More likely, dynein and dynactin act in astrocyte migration via their function in membrane trafficking. In line with this hypothesis, we noticed that the organization of the Golgi apparatus is strongly altered by dynein, dynactin, or GKAP depletion. It is thus tempting to speculate that the key role of dynein in vesicular traffic is essential for migration (Schmoranzer et al., 2003).

Microtubule bending toward the basal membrane is not visible in nonmigrating confluent cells, suggesting that the anchoring mechanism is induced during cell polarization. Wound-induced Cdc42 activation leads to the local recruitment and activation of the Par6–aPKC complex which, in turn, promotes APC clustering at microtubule plus-ends via GSK3β regulation (Etienne-Manneville and Hall, 2003) and independently leads to

Dlg1 recruitment at the cell front (Etienne-Manneville et al., 2005; Fig. 7). Dlg1 colocalizes and interacts with APC at microtubule plus-ends to promote microtubule polarization and centrosome reorientation. We now show that Dlg1 also interacts with dynein and could play a key role in microtubule anchoring at the cell cortex. Dlg1 function in dynein recruitment seems independent of its interaction with APC because APC depletion has a very limited effect on dynein localization on leading edge microtubules. Located at the plus end, APC might play a key role in the initial step of microtubule anchoring at the cell cortex probably by assisting the capture of microtubule plus-ends together with Dlg1. Dlg1-mediated recruitment of dynein could then stabilize microtubule interaction with the cell cortex by generating pulling forces that would prevent microtubule buckling and also promote centrosome forward movement (Fig. 7). In APC-depleted cells, dynein, although recruited on microtubules, may be inactive and unable to couple microtubules to the cell cortex. Dynein activity may be regulated by the positioning of microtubules relative to potential membrane-associated interaction sites. Alternatively, APC could influence dynein activity by modulating Dlg1 conformation. APC binding at the plus ends could also affect the dynactin complex, which localizes at microtubule plus-ends and is required for microtubule anchoring.

Microtubule-mediated forces required for the asymmetric division of the *C. elegans* zygote are also regulated by the Par6–aPKC complex (Grill et al., 2001) and the Cdc42–Par6–aPKC complex is found in a centrosome-attracting body, responsible for asymmetric divisions in the early ascidian embryo (Patalano et al., 2006). It is tempting to speculate that in these models, as in astrocytes, the Cdc42–Par6–aPKC complex locally regulates dynein interaction with microtubules to form a cortical anchoring region from which pulling forces are generated. Discs large, the Dlg1 *Drosophila* orthologue, plays a conserved role in cell polarity (Yamanaka and Ohno, 2008) and our results suggest that it may act downstream of the Par6–aPKC complex to control microtubule network organization through the regulation of dynein-mediated forces.

Loss of GKAP has a severe effect on microtubule organization but does not affect the organization of the Golgi apparatus, suggesting that it is not required for all dynein functions. GKAP rather seems to be specifically involved in loading dynein on the microtubules of the protrusion. During cell migration, GKAP is recruited together with dynein to the cell protrusion in response to the Cdc42-dependent local recruitment of Dlg1. We observe a constitutive interaction between dynein and GKAP, which likely corresponds to their common localization at the centrosome where they also probably interact with Dlg1. It is possible that Dlg1, GKAP, and dynein are brought together at the cell front. However, the interaction between the three proteins appears slightly enhanced during cell migration, as shown by the increased association between Dlg1 and dynein after cell wounding. It has been suggested that APC interaction with Dlg1 could modify the structure of Dlg1 and favor the interaction between GKAP and Dlg1 (Wu et al., 2000). Depletion of APC has a subtle but significant effect on dynein colocalization with microtubules, which may also reflect APC ability to interact with GKAP (Satoh et al., 1997).

Surprisingly, depletion of GKAP or Dlg1 inhibits dynein association with microtubules not only at the plus ends but also all along the microtubules of the protrusion, suggesting that dynein is first recruited to microtubules at the cell front before moving toward the centrosome. Consistently, Dlg1 and GKAP concentrate at the front edge and in the anchoring region. We propose that the anchoring region defines a loading zone where dynein binds to microtubules and initiates its minus-end motor activity.

We have shown here that during cell migration, when the centrosome reorients in the direction of migration and moves forward, dynein associates with leading edge microtubules in the protrusion of migrating cells. Recruitment of dynein and of its regulator dynactin to leading edge microtubules is controlled by the same Cdc42-dependent signaling pathway that is activated at the front of migrating cells. Our results point to dynein association with microtubules as a regulatory mechanism allowing local microtubule anchoring at the cell cortex, generation of asymmetric forces, and subsequent centrosome positioning. Our observations also suggest that upon microtubule network polarization, the microtubule density increases in the protrusive region of the cell. This may contribute to reinforce the forces exerted on the centrosome from the cell front and further stabilize cell polarity. Regulation of microtubule anchoring, associated with this positive feedback, is likely to constitute a fundamental mechanism to control centrosome positioning and, as a consequence, intracellular organization during symmetric and asymmetric cell division, neuronal differentiation, lymphocyte association with its target cell or sheer stress–induced endothelial cell polarization as well as during cell migration.

Materials and methods

Materials

Anti–α-tubulin, anti-Flag, and monoclonal anti-Myc were from Sigma-Aldrich; anti-EB1, monoclonal Dlg1, and anti-p150^{Glued} from Transduction Laboratories; anti-Dlg1 polyclonal from Thermo Fisher Scientific; monoclonal anti-Dlg1 and anti-DHC from Santa Cruz Biotechnology, Inc.; anti-pericentrin and anti-DIC from Covance; anti-GKAP from Covalab; and anti-GFP from Roche. Secondary antibodies were from Jackson ImmunoResearch Laboratories, Inc. Synthetic siRNAs (Invitrogen) correspond to the following sequences: si GKAP-1, 5′-GCUAUCUCAAGGCCACACA-3′; si GKAP-2, 5′-GUCUGGACAGUAUGAAGGC-3′; si GKAP-3, 5′-ACUGAGUUCUGCCGUUGAA-3′; si Scramble, 5′-UCAGAGCUUCGUUGCAGUA-3′; si p150-1, 5′-GGCAAGAACGAUGGUACCG-3′; si p150-2, 5′-UGAGAUGAAUGACGAGCUG-3′; si DHC-1, 5′-GCUCAACACCCAGGAAAUC-3′; si DHC-2, 5′-UGCCAAGUUUAACUACGGC-3′; si EB1-1, 5′-UUCGUUCAAUGGUUCAAGA-3′; si EB1-2, 5′-GAAUAUGAUCCUGUCGCUG-3′; si Cdc42-1, 5′-UGAUGGUGCUGUUGGUAAA-3′; and si Cdc42-2, 5′-GAAUGUGUUUGAUGAAGCA-3′.

Expression constructs

Dlg1 mutant lacking the GUK domain (amino acids 2–927), the C-terminal domain of Dlg1 (Cter, amino acids 545–927), and the GUK domain (amino acids 737–927) were generated by PCR from the initial Dlg1 full-length construct (Etienne-Manneville et al., 2005) subcloned into PRK5-myc. GKAP cDNA (cDNA geneservice, clone ID M5C1043M03) was subcloned in PRK5-flag. GKAP mutants lacking the Dlg1-binding domain (GKAP ΔDlg, lacking the amino acids 191–488) or the LC8-binding domain (GKAP ΔLC8, lacking amino acids 655–688) were generated by PCR engineering.

Cell culture and scratch-induced migration

Culture of primary astrocytes has been previously described in detail (Etienne-Manneville, 2006). For scratch-induced assays, cells were seeded on poly-L-ornithine precoated coverslips or 90-mm-diam dishes, grown in

DME + Glutamax in the presence of serum to confluence and the medium changed 16 h before scratching. Individual wounds (suitable for microinjection and immunofluorescence, around 300 µm wide) were made with a microinjection needle. Wound closure occurred around 16–24 h later. Multiple wounds (suitable for subsequent biochemical analysis) were made with an 8-channel pipette (with 0.1–2 µl tips) scratched several times across the 90-mm dish. Nuclear microinjections in the first row of wound-edge cells were performed immediately after scratching the monolayer. Expression vectors were used at 100–200 µg/ml. Cells were fixed with cold methanol (−20°C, 5 min) or with paraformaldehyde (4% in PBS, 10 min) and permeabilized with Triton X-100 (0.02% in PBS, 10 min). Cells were then stained using standard immunofluorescence techniques. siRNAs were introduced in primary astrocytes by nucleofection (Lonza) following the manufacturer's instructions. COS cells were maintained in DME (Invitrogen) supplemented with 10% FBS at 37°C under a 5% CO_2 atmosphere. Plasmid transfections were performed using the gene juice reagent (VWR) according the manufacturer's instructions.

Imaging

Conventional wide-field epifluorescence images were recorded on a microscope (model DM6000B; Leica) equipped with a 100x HCX Plan Apochromat 1.4 NA objective and a CCD camera (model DFC350FX; Leica) and processed using the Leica Application Suite software. Three TIRF microscopes were used in this study. A home-built variable angle two-color TIRF system described in detail previously (Manneville et al., 2003; Etienne-Manneville et al., 2005) was used to perform quantitative analysis of microtubule z-profiles. In brief, fluorescence was excited either by an Argon ion laser (excitation λ = 488 nm, 25 mW; Melles-Griot) or a Nd:YAG laser (excitation λ = 532 nm, 50 mW; CrystaLaser). The angle of incidence of the excitation light was fixed to 68–70°, above the critical angle θ_c = 61.5°, calculated with $n_i = n_{glass} = 1.52$ and $n_t = n_{culture\ medium} \approx 1.336$ for the refractive indices of the prism and culture medium, respectively. The intensity profile of the evanescent wave is exponentially decaying: $I(z) = I_0\exp(-z/d_P)$, where z is the vertical distance, $I_0 = I(z = 0)$ is the intensity at the interface, and d_P is the penetration depth. The calculated penetration depth for the Argon ion laser was d_P = 75–85 nm and for the Nd:YAG laser was d_P = 85–95 nm. The second TIRF setup, used to acquire immunofluorescence images of fixed cells, was a commercial TIRF system (Olympus) mounted on a microscope (model IX81; Olympus) equipped with a 100x Plan Apochromat 1.45 NA TIRFM objective, an EM CCD camera (iXon+; Andor Technology) and the CellM software (Olympus). The third TIRF microscope was a commercial TIRF system (Carl Zeiss, Inc.) mounted on a microscope (Axiovert 200M; Carl Zeiss, Inc.) driven by MetaMorph software (MDS Analytical Technologies) and equipped with a TIRF 100x Plan Fluar 1.45 NA objective and a CCD camera (Photometrics CoolSNAP HQ2; Roper Industries). Interference reflection microscopy (IRM) was performed on the same setup using the 546-nm wavelength of a 100-W mercury lamp. Live time-lapse phase-contrast videos were also taken on the Carl Zeiss, Inc. TIRF setup at 37°C with a 40x Plan Apochromat 1.3 NA Ph3 objective. Fixed cells were observed at room temperature either in PBS on the TIRF microscopes or mounted in Mowiol on the conventional wide-field epifluorescence microscope.

Live-cell confocal imaging

Astrocytes were electroporated by nucleofection with tubulin-GFP, tubulin-YFP, or EB1-GFP. Time-lapse confocal images were acquired at 0.5–2 frames/s with a microscope (LSM 510; Carl Zeiss, Inc.) equipped with a 63x Plan Apochromat 1.4 NA objective or a microscope (model A1R; Nikon) equipped with a 60x CFI Plan Apochromat VC 1.4 NA objective at 37°C in culture medium supplemented with 20 mM Hepes. To visualize EB1 dynamics, composite images were generated by superimposing image N (color coded in green) with image N+1 (color coded in red) using the Add function in MetaMorph. The two frames were separated by a time interval, Δt = 1.2–1.9 s, depending on the acquisition rate. In control cells, red EB1 spots position are in front of the corresponding green EB1 spot toward the cell leading edge. In siRNA-treated cells in which microtubule dynamics are perturbed, red spots are found on the side or behind (relative to the cell leading edge) the corresponding green spot.

Image quantification

Image processing was performed using Optimas 6.5 (Media Cybernetics), MetaMorph, and ImageJ (NIH, Bethesda, MD).

Microtubule z-profiles. To assess microtubule proximity to the plasma membrane, we superimposed the TIRF image of cells fixed 8 h after wounding and stained with antibodies directed against tubulin with the corresponding wide-field epifluorescence (Epi) image. Because of the exponential decay of the evanescent field, the TIRF image shows signal from proteins localized within $\sim 3 \times d_P \sim 300$ nm from the basal plasma membrane—corresponding to a 100-fold decrease in light intensity—and greatly enhances the fluorescence close (<100 nm) to the plasma membrane. In the case of a "bent" microtubule that spans the entire evanescent field, the gain of the camera was adjusted so that the fluorescence of the brightest point was not saturated.

To get a quantitative 3D view of the organization of the microtubule cytoskeleton, we have used the theoretical relationship between the fluorescence intensity and the vertical position to determine the height profile ("z-profile") $z(r)$ of microtubules according to

$$z(r) = -d_P \ln \frac{I(r)}{I\max},$$

where $I(r)$ is the fluorescence intensity along the microtubule at a distance r from the leading edge of the cell and I_{max} is the fluorescence of the brightest point in the image. Note that vertical measurements are not absolute distances but relative to the lowest point in the image (z = 0 for $I = I_{max}$). The cell-averaged z-profile was obtained as follows. From each average microtubule z-profile, the x, y, and z positions of five points were determined: the microtubule plus-end, the lowest point in the profile, the start and end points of the "contact" zone defined as being within 5 nm above the lowest point, and the point furthest from the leading edge and still visible in TIRF. The positions of these five points were then averaged.

We define cells with polarized microtubule z-profiles as cells in which microtubules approach the substrate only at the front of the cell. In TIRF illumination mode, such cells show a characteristic increase in tubulin fluorescence near the leading edge. In contrast, in a cell with nonpolarized microtubule z-profiles, microtubules are visible throughout the cell footprint.

Colocalization of DIC and microtubules. Images were first filtered using the Flatten Background function in MetaMorph and a region of interest containing the cell was selected. The Measure Colocalization function was then applied to determine the percentage of DIC localizing on microtubules. In control nontreated or siRNA GFP–depleted cells (Ctl), colocalization of DIC on microtubules was 53 ± 3% (n = 19). A scrambled negative control (Ctl rotated) was obtained from control cells by rotating the microtubule image by 1°, giving a random colocalization of 18 ± 1% (n = 19). Colocalization of vinculin with microtubules, used as an additional negative control, was 25 ± 1% (n = 21). Data were normalized to control conditions by setting positive control colocalization to 100% and negative control random colocalization (Ctl rotated) to 0%. n = 23, 16, 3, 38, 14, and 19 cells were scored in si Cdc42–, si APC–, si EB1–, si Dlg1–, si GKAP 1–, and si GKAP 2–treated cells, respectively. To visualize colocalization, a binary mask was created using the AND operation in MetaMorph applied to the thresholded and binarized images of DIC (or vinculin) and microtubule stainings.

Combined IRM and dual-color TIRF imaging. The Intensity Plot function in ImageJ was used to measure gray level intensities of the IRM image and of the inverted fluorescence intensities of microtubule and actin stainings. Low gray levels in IRM reflect strong adhesion and closer proximity of the membrane to the substrate. Similarly, because fluorescence signals were inverted, low actin or microtubule signals correspond to a higher proximity with the plasma membrane.

Centrosome and Golgi apparatus reorientation. Centrosome and Golgi apparatus reorientation was determined as described previously (Etienne-Manneville, 2006). In brief, 8 h after wounding, astrocytes were fixed and stained with anti-pericentrin (centrosome), anti-GM130 (Golgi apparatus), Hoechst (nucleus), and anti-myc when necessary. Cells in which the centrosome or the Golgi apparatus was within the quadrant facing the wound (±45° deviation from the direction perpendicular to the wound) were scored as polarized. For each point at least 100 cells from three independent experiments were examined. Because random polarization is 25% in our assay, data were normalized to control conditions by subtracting random orientation (25%) and by setting reorientation to 100% for cells treated by a control siRNA directed against GFP (si GFP). Non-normalized raw data are presented in Fig. S2, D and E, and Fig. S5.

DIC, Dlg1, and GKAP immunofluorescence in, respectively, DHC-, Dlg1-, and GKAP siRNA–depleted cells. The Measure Intensity function in ImageJ was used to measure the fluorescence intensity from a region of interest drawn around wound-edge cells and from a region of interest in front of the cells used as a background signal. The background signal was subtracted. Data from 20–40 fields containing 3–6 cells were averaged and normalized by the control condition.

EB1-GFP cluster dynamics. The Matlab MatPIV toolbox for Particle Image Velocimetry (downloadable from http://folk.uio.no/jks/matpiv/index2.html) was used to determine the velocity vectors of EB1-GFP clusters between two consecutive frames. The angle between the velocity vectors and the direction of migration was then calculated. To quantify the percentage of abnormal EB1 dynamics, the videos were segmented into 20-s time intervals. From these segments, seven frames were overlaid using the MetaMorph Overlay function to obtain a rainbow color-coded time projection. Abnormal EB1 dynamics showed up as bent and/or inversely colored tracks and were then easily counted manually. 70–264 EB1 clusters were counted throughout each video.

Immunoprecipitation

Cells were washed with ice-cold PBS containing 1 mM orthovanadate and were lysed at 4°C in Nonidet P-40 buffer (10 mM Tris/HCl, pH 7.5, 140 mM NaCl, 1 mM orthovanadate and 1% Nonidet P-40, 2 mM PMSF, 5 mM EDTA, and protease inhibitor mix from Roche). Nuclei were discarded after centrifugation at 10,000 *g* for 10 min. Lysates were incubated overnight at 4°C with indicated antibodies protein G–Sepharose. Immunoprecipitates were collected by centrifugation and extensively washed in Nonidet P-40 buffer. Immunoprecipitated proteins were eluted with SDS-sample buffer and analyzed by 7.5% SDS-PAGE.

Online supplemental material

Fig. S1 shows the depletion of DHC, p150, Cdc42, and EB1 by siRNA. Fig. S2 shows that the dynein–dynactin complex controls centrosome and Golgi reorientation. Fig. S3 shows the quantification of EB1-GFP dynamics in DHC-, Dlg1-, and GKAP-depleted cells compared with control cells. Fig. S4 shows the interaction between GKAP and Dlg1. Fig. S5 shows that GKAP is required for centrosome reorientation. Videos 1 and 2 show microtubule dynamics in control migrating astrocytes. Videos 3 and 4 show the migration of astrocytes with phase-contrast and IRM, respectively. Video 5 shows microtubule dynamics in a DHC-depleted astrocyte. Videos 6–10 show the dynamics of EB1-GFP in control, si GFP–, si DHC–, si Dlg1–, and si GKAP–treated astrocytes, respectively. All videos, except Video 3 (phase-contrast) and Video 4 (IRM), were acquired by confocal microscopy. Online supplemental material is available at http://www.jcb.org/cgi/content/full/jcb.201002151/DC1.

We would like to thank Mike Ferenczi, Bruno Goud, the Imaging platform at Institut Pasteur and Nathalie Sauvonet, the Imaging Platform at Institut Curie, and the Nikon Imaging Center at Institut Curie for their technical support.

This work was supported by the Centre National de la Recherche Scientifique, the Institut Pasteur, the Fondation de France, the Institut pour la Recherche sur la Moelle Épinière et l'Encéphale, and La Ligue Contre le Cancer. S. Etienne-Manneville is a member of the EMBO Young Investigator Program.

Submitted: 28 February 2010
Accepted: 5 October 2010

References

Allan, V.J., H.M. Thompson, and M.A. McNiven. 2002. Motoring around the Golgi. *Nat. Cell Biol.* 4:E236–E242. doi:10.1038/ncb1002-e236

Axelrod, D. 2001. Total internal reflection fluorescence microscopy in cell biology. *Traffic.* 2:764–774. doi:10.1034/j.1600-0854.2001.21104.x

Burakov, A., E. Nadezhdina, B. Slepchenko, and V. Rodionov. 2003. Centrosome positioning in interphase cells. *J. Cell Biol.* 162:963–969. doi:10.1083/jcb.200305082

Carminati, J.L., and T. Stearns. 1997. Microtubules orient the mitotic spindle in yeast through dynein-dependent interactions with the cell cortex. *J. Cell Biol.* 138:629–641. doi:10.1083/jcb.138.3.629

Combs, J., S.J. Kim, S. Tan, L.A. Ligon, E.L. Holzbaur, J. Kuhn, and M. Poenie. 2006. Recruitment of dynein to the Jurkat immunological synapse. *Proc. Natl. Acad. Sci. USA.* 103:14883–14888. doi:10.1073/pnas.0600914103

Corellou, F., S.M. Coelho, F.Y. Bouget, and C. Brownlee. 2005. Spatial reorganisation of cortical microtubules in vivo during polarisation and asymmetric division of Fucus zygotes. *J. Cell Sci.* 118:2723–2734. doi:10.1242/jcs.02353

Cowan, C.R., and A.A. Hyman. 2004. Asymmetric cell division in *C. elegans*: cortical polarity and spindle positioning. *Annu. Rev. Cell Dev. Biol.* 20:427–453. doi:10.1146/annurev.cellbio.19.111301.113823

Daga, R.R., A. Yonetani, and F. Chang. 2006. Asymmetric microtubule pushing forces in nuclear centering. *Curr. Biol.* 16:1544–1550. doi:10.1016/j.cub.2006.06.026

de Anda, F.C., G. Pollarolo, J.S. Da Silva, P.G. Camoletto, F. Feiguin, and C.G. Dotti. 2005. Centrosome localization determines neuronal polarity. *Nature.* 436:704–708. doi:10.1038/nature03811

Dogterom, M., J.W. Kerssemakers, G. Romet-Lemonne, and M.E. Janson. 2005. Force generation by dynamic microtubules. *Curr. Opin. Cell Biol.* 17:67–74. doi:10.1016/j.ceb.2004.12.011

Dujardin, D.L., L.E. Barnhart, S.A. Stehman, E.R. Gomes, G.G. Gundersen, and R.B. Vallee. 2003. A role for cytoplasmic dynein and LIS1 in directed cell movement. *J. Cell Biol.* 163:1205–1211. doi:10.1083/jcb.200310097

Eshel, D., L.A. Urrestarazu, S. Vissers, J.C. Jauniaux, J.C. van Vliet-Reedijk, R.J. Planta, and I.R. Gibbons. 1993. Cytoplasmic dynein is required for normal nuclear segregation in yeast. *Proc. Natl. Acad. Sci. USA.* 90:11172–11176. doi:10.1073/pnas.90.23.11172

Etienne-Manneville, S. 2004. Cdc42—the centre of polarity. *J. Cell Sci.* 117:1291–1300. doi:10.1242/jcs.01115

Etienne-Manneville, S. 2006. In vitro assay of primary astrocyte migration as a tool to study Rho GTPase function in cell polarization. *Methods Enzymol.* 406:565–578. doi:10.1016/S0076-6879(06)06044-7

Etienne-Manneville, S., and A. Hall. 2001. Integrin-mediated activation of Cdc42 controls cell polarity in migrating astrocytes through PKCzeta. *Cell.* 106:489–498. doi:10.1016/S0092-8674(01)00471-8

Etienne-Manneville, S., and A. Hall. 2003. Cdc42 regulates GSK-3beta and adenomatous polyposis coli to control cell polarity. *Nature.* 421:753–756. doi:10.1038/nature01423

Etienne-Manneville, S., J.B. Manneville, S. Nicholls, M.A. Ferenczi, and A. Hall. 2005. Cdc42 and Par6-PKCzeta regulate the spatially localized association of Dlg1 and APC to control cell polarization. *J. Cell Biol.* 170:895–901. doi:10.1083/jcb.200412172

Faivre-Moskalenko, C., and M. Dogterom. 2002. Dynamics of microtubule asters in microfabricated chambers: the role of catastrophes. *Proc. Natl. Acad. Sci. USA.* 99:16788–16793. doi:10.1073/pnas.252407099

Felgner, H., R. Frank, and M. Schliwa. 1996. Flexural rigidity of microtubules measured with the use of optical tweezers. *J. Cell Sci.* 109:509–516.

Fujita, A., and Y. Kurachi. 2000. SAP family proteins. *Biochem. Biophys. Res. Commun.* 269:1–6. doi:10.1006/bbrc.1999.1893

Gomes, E.R., S. Jani, and G.G. Gundersen. 2005. Nuclear movement regulated by Cdc42, MRCK, myosin, and actin flow establishes MTOC polarization in migrating cells. *Cell.* 121:451–463. doi:10.1016/j.cell.2005.02.022

Gönczy, P., S. Pichler, M. Kirkham, and A.A. Hyman. 1999. Cytoplasmic dynein is required for distinct aspects of MTOC positioning, including centrosome separation, in the one cell stage *Caenorhabditis elegans* embryo. *J. Cell Biol.* 147:135–150. doi:10.1083/jcb.147.1.135

Grabham, P.W., G.E. Seale, M. Bennecib, D.J. Goldberg, and R.B. Vallee. 2007. Cytoplasmic dynein and LIS1 are required for microtubule advance during growth cone remodeling and fast axonal outgrowth. *J. Neurosci.* 27:5823–5834. doi:10.1523/JNEUROSCI.1135-07.2007

Grill, S.W., and A.A. Hyman. 2005. Spindle positioning by cortical pulling forces. *Dev. Cell.* 8:461–465. doi:10.1016/j.devcel.2005.03.014

Grill, S.W., P. Gönczy, E.H. Stelzer, and A.A. Hyman. 2001. Polarity controls forces governing asymmetric spindle positioning in the *Caenorhabditis elegans* embryo. *Nature.* 409:630–633. doi:10.1038/35054572

Grill, S.W., J. Howard, E. Schäffer, E.H. Stelzer, and A.A. Hyman. 2003. The distribution of active force generators controls mitotic spindle position. *Science.* 301:518–521. doi:10.1126/science.1086560

Harada, A., Y. Takei, Y. Kanai, Y. Tanaka, S. Nonaka, and N. Hirokawa. 1998. Golgi vesiculation and lysosome dispersion in cells lacking cytoplasmic dynein. *J. Cell Biol.* 141:51–59. doi:10.1083/jcb.141.1.51

Holy, T.E., M. Dogterom, B. Yurke, and S. Leibler. 1997. Assembly and positioning of microtubule asters in microfabricated chambers. *Proc. Natl. Acad. Sci. USA.* 94:6228–6231. doi:10.1073/pnas.94.12.6228

Hyman, A.A., and E. Karsenti. 1996. Morphogenetic properties of microtubules and mitotic spindle assembly. *Cell.* 84:401–410. doi:10.1016/S0092-8674(00)81285-4

Keays, D.A., G. Tian, K. Poirier, G.J. Huang, C. Siebold, J. Cleak, P.L. Oliver, M. Fray, R.J. Harvey, Z. Molnár, et al. 2007. Mutations in alpha-tubulin cause abnormal neuronal migration in mice and lissencephaly in humans. *Cell.* 128:45–57. doi:10.1016/j.cell.2006.12.017

Kim, E., S. Naisbitt, Y.P. Hsueh, A. Rao, A. Rothschild, A.M. Craig, and M. Sheng. 1997. GKAP, a novel synaptic protein that interacts with the guanylate kinase-like domain of the PSD-95/SAP90 family of channel clustering molecules. *J. Cell Biol.* 136:669–678. doi:10.1083/jcb.136.3.669

Kimura, A., and S. Onami. 2007. Local cortical pulling-force repression switches centrosomal centration and posterior displacement in *C. elegans*. *J. Cell Biol.* 179:1347–1354. doi:10.1083/jcb.200706005

King, S.M. 2003. Organization and regulation of the dynein microtubule motor. *Cell Biol. Int.* 27:213–215. doi:10.1016/S1065-6995(02)00337-2

Kirschner, M., and T. Mitchison. 1986. Beyond self-assembly: from microtubules to morphogenesis. *Cell.* 45:329–342. doi:10.1016/0092-8674(86)90318-1

Komarova, Y., C.O. De Groot, I. Grigoriev, S.M. Gouveia, E.L. Munteanu, J.M. Schober, S. Honnappa, R.M. Buey, C.C. Hoogenraad, M. Dogterom, et al. 2009. Mammalian end binding proteins control persistent microtubule growth. *J. Cell Biol.* 184:691–706. doi:10.1083/jcb.200807179

Koonce, M.P., and M. Samsó. 2004. Of rings and levers: the dynein motor comes of age. *Trends Cell Biol.* 14:612–619. doi:10.1016/j.tcb.2004.09.013

Koonce, M.P., J. Köhler, R. Neujahr, J.-M. Schwartz, I. Tikhonenko, and G. Gerisch. 1999. Dynein motor regulation stabilizes interphase microtubule arrays and determines centrosome position. *EMBO J.* 18:6786–6792. doi:10.1093/emboj/18.23.6786

Kosako, H., M. Amano, M. Yanagida, K. Tanabe, Y. Nishi, K. Kaibuchi, and M. Inagaki. 1997. Phosphorylation of glial fibrillary acidic protein at the same sites by cleavage furrow kinase and Rho-associated kinase. *J. Biol. Chem.* 272:10333–10336. doi:10.1074/jbc.272.16.10333

Krylyshkina, O., K.I. Anderson, I. Kaverina, I. Upmann, D.J. Manstein, J.V. Small, and D.K. Toomre. 2003. Nanometer targeting of microtubules to focal adhesions. *J. Cell Biol.* 161:853–859. doi:10.1083/jcb.200301102

Li, M., M. McGrail, M. Serr, and T.S. Hays. 1994. *Drosophila* cytoplasmic dynein, a microtubule motor that is asymmetrically localized in the oocyte. *J. Cell Biol.* 126:1475–1494. doi:10.1083/jcb.126.6.1475

Manneville, J.B., and S. Etienne-Manneville. 2006. Positioning centrosomes and spindle poles: looking at the periphery to find the centre. *Biol. Cell.* 98:557–565. doi:10.1042/BC20060017

Manneville, J.B., S. Etienne-Manneville, P. Skehel, T. Carter, D. Ogden, and M. Ferenczi. 2003. Interaction of the actin cytoskeleton with microtubules regulates secretory organelle movement near the plasma membrane in human endothelial cells. *J. Cell Sci.* 116:3927–3938. doi:10.1242/jcs.00672

Markus, S.M., J.J. Punch, and W.L. Lee. 2009. Motor- and tail-dependent targeting of dynein to microtubule plus ends and the cell cortex. *Curr. Biol.* 19:196–205. doi:10.1016/j.cub.2008.12.047

Niclas, J., V.J. Allan, and R.D. Vale. 1996. Cell cycle regulation of dynein association with membranes modulates microtubule-based organelle transport. *J. Cell Biol.* 133:585–593. doi:10.1083/jcb.133.3.585

Oiwa, K., and H. Sakakibara. 2005. Recent progress in dynein structure and mechanism. *Curr. Opin. Cell Biol.* 17:98–103. doi:10.1016/j.ceb.2004.12.006

Osmani, N., N. Vitale, J.P. Borg, and S. Etienne-Manneville. 2006. Scrib controls Cdc42 localization and activity to promote cell polarization during astrocyte migration. *Curr. Biol.* 16:2395–2405. doi:10.1016/j.cub.2006.10.026

Palazzo, A.F., H.L. Joseph, Y.J. Chen, D.L. Dujardin, A.S. Alberts, K.K. Pfister, R.B. Vallee, and G.G. Gundersen. 2001. Cdc42, dynein, and dynactin regulate MTOC reorientation independent of Rho-regulated microtubule stabilization. *Curr. Biol.* 11:1536–1541. doi:10.1016/S0960-9822(01)00475-4

Patalano, S., G. Prulière, F. Prodon, A. Paix, P. Dru, C. Sardet, and J. Chenevert. 2006. The aPKC-PAR-6-PAR-3 cell polarity complex localizes to the centrosome attracting body, a macroscopic cortical structure responsible for asymmetric divisions in the early ascidian embryo. *J. Cell Sci.* 119:1592–1603. doi:10.1242/jcs.02873

Peng, H., W. Shah, P. Holland, and S. Carbonetto. 2008. Integrins and dystroglycan regulate astrocyte wound healing: the integrin beta1 subunit is necessary for process extension and orienting the microtubular network. *Dev. Neurobiol.* 68:559–574. doi:10.1002/dneu.20593

Peris, L., M. Wagenbach, L. Lafanechère, J. Brocard, A.T. Moore, F. Kozielski, D. Job, L. Wordeman, and A. Andrieux. 2009. Motor-dependent microtubule disassembly driven by tubulin tyrosination. *J. Cell Biol.* 185:1159–1166. doi:10.1083/jcb.200902142

Reinsch, S., and E. Karsenti. 1997. Movement of nuclei along microtubules in *Xenopus* egg extracts. *Curr. Biol.* 7:211–214. doi:10.1016/S0960-9822(97)70092-7

Rodríguez-Crespo, I., B. Yélamos, F. Roncal, J.P. Albar, P.R. Ortiz de Montellano, and F. Gavilanes. 2001. Identification of novel cellular proteins that bind to the LC8 dynein light chain using a pepscan technique. *FEBS Lett.* 503:135–141. doi:10.1016/S0014-5793(01)02718-1

Roghi, C., and V.J. Allan. 1999. Dynamic association of cytoplasmic dynein heavy chain 1a with the Golgi apparatus and intermediate compartment. *J. Cell Sci.* 112:4673–4685.

Sasaki, S., A. Shionoya, M. Ishida, M.J. Gambello, J. Yingling, A. Wynshaw-Boris, and S. Hirotsune. 2000. A LIS1/NUDEL/cytoplasmic dynein heavy chain complex in the developing and adult nervous system. *Neuron.* 28:681–696. doi:10.1016/S0896-6273(00)00146-X

Satoh, K., H. Yanai, T. Senda, K. Kohu, T. Nakamura, N. Okumura, A. Matsumine, S. Kobayashi, K. Toyoshima, and T. Akiyama. 1997. DAP-1, a novel protein that interacts with the guanylate kinase-like domains of hDLG and PSD-95. *Genes Cells.* 2:415–424. doi:10.1046/j.1365-2443.1997.1310329.x

Schmoranzer, J., G. Kreitzer, and S.M. Simon. 2003. Migrating fibroblasts perform polarized, microtubule-dependent exocytosis towards the leading edge. *J. Cell Sci.* 116:4513–4519. doi:10.1242/jcs.00748

Segal, M., and K. Bloom. 2001. Control of spindle polarity and orientation in *Saccharomyces cerevisiae*. *Trends Cell Biol.* 11:160–166. doi:10.1016/S0962-8924(01)01954-7

Sheeman, B., P. Carvalho, I. Sagot, J. Geiser, D. Kho, M.A. Hoyt, and D. Pellman. 2003. Determinants of *S. cerevisiae* dynein localization and activation: implications for the mechanism of spindle positioning. *Curr. Biol.* 13:364–372. doi:10.1016/S0960-9822(03)00013-7

Shu, T., R. Ayala, M.D. Nguyen, Z. Xie, J.G. Gleeson, and L.H. Tsai. 2004. Ndel1 operates in a common pathway with LIS1 and cytoplasmic dynein to regulate cortical neuronal positioning. *Neuron.* 44:263–277. doi:10.1016/j.neuron.2004.09.030

Siegrist, S.E., and C.Q. Doe. 2006. Extrinsic cues orient the cell division axis in *Drosophila* embryonic neuroblasts. *Development.* 133:529–536. doi:10.1242/dev.02211

Skop, A.R., and J.G. White. 1998. The dynactin complex is required for cleavage plane specification in early *Caenorhabditis elegans* embryos. *Curr. Biol.* 8:1110–1116. doi:10.1016/S0960-9822(98)70465-8

Solecki, D.J., L. Model, J. Gaetz, T.M. Kapoor, and M.E. Hatten. 2004. Par6alpha signaling controls glial-guided neuronal migration. *Nat. Neurosci.* 7:1195–1203. doi:10.1038/nn1332

Stinchcombe, J.C., E. Majorovits, G. Bossi, S. Fuller, and G.M. Griffiths. 2006. Centrosome polarization delivers secretory granules to the immunological synapse. *Nature.* 443:462–465. doi:10.1038/nature05071

Straube, A., and A. Merdes. 2007. EB3 regulates microtubule dynamics at the cell cortex and is required for myoblast elongation and fusion. *Curr. Biol.* 17:1318–1325. doi:10.1016/j.cub.2007.06.058

Tanaka, T., F.F. Serneo, C. Higgins, M.J. Gambello, A. Wynshaw-Boris, and J.G. Gleeson. 2004. Lis1 and doublecortin function with dynein to mediate coupling of the nucleus to the centrosome in neuronal migration. *J. Cell Biol.* 165:709–721. doi:10.1083/jcb.200309025

Tawil, N.J., P. Wilson, and S. Carbonetto. 1994. Expression and distribution of functional integrins in rat CNS glia. *J. Neurosci. Res.* 39:436–447. doi:10.1002/jnr.490390411

Tolić-Nørrelykke, I.M. 2008. Push-me-pull-you: how microtubules organize the cell interior. *Eur. Biophys. J.* 37:1271–1278. doi:10.1007/s00249-008-0321-0

Tolić-Nørrelykke, I.M., L. Sacconi, G. Thon, and F.S. Pavone. 2004. Positioning and elongation of the fission yeast spindle by microtubule-based pushing. *Curr. Biol.* 14:1181–1186. doi:10.1016/j.cub.2004.06.029

Toomre, D., and D.J. Manstein. 2001. Lighting up the cell surface with evanescent wave microscopy. *Trends Cell Biol.* 11:298–303. doi:10.1016/S0962-8924(01)02027-X

Tsai, L.-H., and J.G. Gleeson. 2005. Nucleokinesis in neuronal migration. *Neuron.* 46:383–388. doi:10.1016/j.neuron.2005.04.013

Tsai, J.W., K.H. Bremner, and R.B. Vallee. 2007. Dual subcellular roles for LIS1 and dynein in radial neuronal migration in live brain tissue. *Nat. Neurosci.* 10:970–979. doi:10.1038/nn1934

Vallee, R.B., and S.A. Stehman. 2005. How dynein helps the cell find its center: a servomechanical model. *Trends Cell Biol.* 15:288–294. doi:10.1016/j.tcb.2005.04.005

Wu, H., C. Reissner, S. Kuhlendahl, B. Coblentz, S. Reuver, S. Kindler, E.D. Gundelfinger, and C.C. Garner. 2000. Intramolecular interactions regulate SAP97 binding to GKAP. *EMBO J.* 19:5740–5751. doi:10.1093/emboj/19.21.5740

Wynshaw-Boris, A., and M.J. Gambello. 2001. LIS1 and dynein motor function in neuronal migration and development. *Genes Dev.* 15:639–651. doi:10.1101/gad.886801

Yamanaka, T., and S. Ohno. 2008. Role of Lgl/Dlg/Scribble in the regulation of epithelial junction, polarity and growth. *Front. Biosci.* 13:6693–6707. doi:10.2741/3182

Yvon, A.M., J.W. Walker, B. Danowski, C. Fagerstrom, A. Khodjakov, and P. Wadsworth. 2002. Centrosome reorientation in wound-edge cells is cell type specific. *Mol. Biol. Cell.* 13:1871–1880. doi:10.1091/mbc.01-11-0539